Journal of Power Sources 605 (2024) 234481

Contents lists available at ScienceDirect

Journal of Power Sources

journal homepage: www.elsevier.com/locate/jpowsour

Operando GC/MS for the investigation of different decomposition pathways during solid electrolyte interphase (SEI) formation with SEI forming additives

Christiane Groher [a], Damian Marlon Cupid [a], Andreas Mautner [b,c], Erwin Rosenberg [d], Jürgen Kahr [a,*]

[a] AIT Austrian Institute of Technology GmbH, Center for Low-Emission Transport, Battery Technologies, Giefinggasse 2, 1210, Vienna, Austria
[b] Institute of Environmental Biotechnology, IFA-Tulln, University of Natural Resources and Life Sciences Vienna, Konrad-Lorenz-Straße 20, 3430, Tulln an der Donau, Austria
[c] Institute of Materials Chemistry & Research, Faculty of Chemistry, University of Vienna, Währinger Straße 42, 1090, Vienna, Austria
[d] Vienna University of Technology, Institute of Chemical Technologies and Analytics, Getreidemarkt 9/164 AC, 1060, Vienna, Austria

HIGHLIGHTS

- Solid electrolyte interphase and cathode electrolyte interphase investigation.
- Comparison of SEI forming additives VC and FEC.
- Analysis of complex gas mixture from electrolyte decomposition.
- Decomposition pathways investigated by operando GC/MS and XPS.

ABSTRACT

The interphases on the electrodes that form from electrolyte decomposition play a crucial role in the battery performance. However, with a thickness of only a few nanometres the formed passivation layers present a challenge to explore. In this work, we implemented a new approach by combining operando GC/MS gas analysis supported by surface sensitive XPS to investigate the electrolyte decomposition during SEI formation and deepen the understanding of the decomposition reactions of vinylene carbonate (VC) and fluoroethylene carbonate (FEC). Electrolyte degradation results in the formation of 29 different gas species. Adding additives resulted in (i) reduced gas formation and (ii) a clear shift from hydrocarbons to carbon oxides. Carbon dioxide was found to be indicative of the formation of poly-VC which was supported by findings from post-mortem XPS. An increased amount of fluorine was found in the interphases of cells using FEC as electrolyte additive. Acetaldehyde was identified as gaseous component to differentiate the decomposition of VC and FEC. For the decomposition of the base electrolyte components ethylene carbonate (EC) and diethyl carbonate (DEC), methane, ethane, ethene and butane were found to be indicative, and a scavenging effect of VC for alkoxides was confirmed by monitoring ethanol.

1. Introduction

Since their commercialization in 1991 by Sony the demand for lithium-ion batteries (LIBs) has skyrocketed. This is due to the heightened political and societal awareness of electric vehicles (EVs) as solutions for climate-neutral transport, increased EV production, and LIB demand for energy storage and load-levelling solutions. LIB research is driven by the need to develop active materials and components can be used to fabricate cells with increased specific capacity, volumetric energy density, cycle life, and safety. Emphasis is placed on understanding the structural changes of the active materials during cycling, interphase formation reactions, and cell degradation mechanisms [1–3] The development of LIBs as we know them today was enabled by the discovery of carbon-based anodes in combination with cyclic carbonate electrolytes. This carbonate electrolyte, along with the conductive salt, forms a passivation layer on the negative electrode which inhibits further reaction between electrode and electrolyte. This Solid Electrolyte Interphase (SEI) is an electronically insulating layer which allows Li-ions to pass through and intercalate into the negative electrode, commonly graphite. The interphase forms mainly during the first charge

* Corresponding author.
E-mail address: juergen.kahr@ait.ac.at (J. Kahr).

https://doi.org/10.1016/j.jpowsour.2024.234481
Received 15 November 2023; Received in revised form 22 March 2024; Accepted 30 March 2024
Available online 17 April 2024

cycle of the cell and is accompanied by a non-reversible initial capacity loss [4–6]. The SEI layer with a thickness of approximately 10 nm consists of an inorganic part located closer to the electrode surface and an organic portion that extends into the electrolyte. Most research focuses on the combination of a graphitic anode and carbonate-based electrolytes, usually containing the cyclic ethylene carbonate (EC). In such cases, the inorganic SEI contains LiF, Li_2CO_3, LiOH and Li_2O [1,7]. The organic part is more complex and its composition depends on the electrolyte and used additives. Dimethylcarbonate (DMC) leads mainly to the formation of the oligomeric species dimethyl 2,5-dioxahexane dicarboxylate (DMDOHC) whereas diethyl 2,5-dioxahexane dicarboxylate (DEDOHC) is formed when diethylcarbonate (DEC) is used as an electrolyte component. In general, the organic part of the SEI can be described as a mix of polymeric and oligomeric decomposition products of the electrolyte [7,8].

Even though the SEI should prevent electrolyte decomposition during subsequent cycling, due to the expansion of the electrode material during Li^+-insertion small cracks are formed which expose fresh electrode surfaces to the electrolyte, thereby leading to further electrolyte decomposition and capacity fading [9]. This led to the development of SEI forming additives like vinylene carbonate (VC) and fluoroethylene carbonate (FEC), which are structurally similar to EC (see Fig. S1) but decompose earlier on the negative electrode upon charging [10]. It was shown that VC and FEC form thinner interphases containing poly-VC in the organic part, which increase the elasticity of the SEI and therefore lowered capacity loss due to reduced crack formation. During cell aging, polyethylene glycol (PEO) is formed in the SEI. The amount of PEO can be used as an indicator of the quality of the SEI, since continuous decomposition of the electrolyte yields a larger amount of the polymer. In cells with VC or FEC, less PEO is detected on the electrode surface after cell aging [11–13]. Generally 2–3 wt% of additives are used in electrolyte formulations.

The cathode electrolyte interphase (CEI), which forms on the positive electrode is the less understood pendant to the SEI. In contrast to the SEI, which is formed from the reductive decomposition products of the electrolyte, the growth of the CEI involves oxidative processes. Although the surface species on the CEI are similar to those in the SEI [11,12,14–18], the CEI is usually thinner (1–2 nm), and some reports claim that there is only a partial coverage of the positive electrode [12,16,19]. Although typical electrolyte formulations use 2–3 wt% of additives, in some cases, higher concentrations may be used. However, this can lead to increased electrolyte decomposition on the cathode side, thereby resulting in higher cell impedances [20].

The SEI is a dynamic and therefore continuously evolving system. Thus, investigating its composition during cell operation is of paramount interest. Only a few approaches in that regard can be found and currently available data stems mainly from post-mortem analysis and simulations based on mathematical models [21]. Post-mortem investigations are primarily performed with surface sensitive techniques such as X-Ray Photoelectron Spectroscopy (XPS) or Transmission Electron Microscopy (TEM). On the other hand, monitoring the gas phase with an *operando* system provides the possibility of deciphering the decomposition reactions that lead to SEI formation during cell operation. The first gas analyses estimated the amount of formed gas by using thickness measurements and volume expansion via the Archimedes principle [22]. In another study, the gas phase was investigated by penetrating the closed space of a battery with a syringe to extract a gas sample and analysing this sample with gas chromatography [23]. Finally, in-situ data can be collected with Online Electrochemical Mass Spectrometer (OEMS) gaining information on the gas development in a working battery cell. The OEMS is a device that flushes a cell with a carrier gas, which is then investigated via mass spectrometry. Using this method, one particular mass significant for a gas species can be monitored, or a mathematical model can be used to deconvolute the fragmented mass spectrum significant for the analyte [24–26]. However, this online gas analysis is limited to monitoring only a few gasses simultaneously. In this paper we add a gas chromatograph (GC) to separate the gas mixture before entering the mass spectrometer (MS). Therefore, a full qualitative analysis of the gas phase including gas species that are beyond the reach of OEMS can be performed, and semi-quantitative information of trace components in the gas phase can be attained.

Table 1
Electrode material compositions.

	Negative Electrode	Positive Electrode
Active material	95 % Graphite material (HED graphite 918-A2; d50 = 14.93 µm) *Targray Technology International Inc, Kirkland, QC, Canada;*	92 % NMC 811 (uncoated) *Targray*
Carbon Black	2 % Super 65 Carbon Black *Imerys SA, Paris, France*	4 % Super 65 Carbon Black *Imerys SA*
Binder	• 2 % CMC (Carboxymethyl Cellulose) (WALOCEL™ CRT 2000 WPA) *DuPont de Nemours Inc., Wilmington, DE, USA* • 1 % Styrene-butadiene latex *JSR Corporation, Tokyo, Japan*	4 % PVDF *Solef, Solvay SA, Brussels, Belgium*
Solvent	Purified water	NMP (N-methyl-pyrrolidone, ≥99.8 %) *VWR chemicals, Solon, Ohio, USA*

This paper uses a combination of *operando* GC/MS and post-mortem XPS to investigate electrolyte decomposition and SEI formation in cells with NMC811 vs. graphite in 1 M $LiPF_6$ EC/DEC 1:1 without (Ref) and with 1 wt% additive (VC and FEC). Here we show that *operando* GC/MS is suitable to detect small changes in the electrolyte composition via the gaseous decomposition products and can therefore be used to investigate the effect of electrolyte additives even at concentrations of only 1 wt%. With the increased sensitivity and dynamic range of the *operando* GC/MS, it is possible to elucidate and confirm reactions that remain concealed to OEMS analysis as the technique cannot be used to monitor larger molecules with a more complex fragmentation pattern.

2. Methods and materials

2.1. Electrode preparation

The electrodes for the NMC811 vs. graphite cells were prepared in-house on a roll-to-roll coating machine (SC 30, Coatema Coating Machinery GmbH, Dormagen, Germany). The slurries were prepared in a high-energy disperser (DISPERMAT CV3-PLUS, VMA GETZMANN GmbH, Reichsdorf, Germany) with the compositions listed in Table 1. The slurry of the positive electrode was coated on an Al foil (22 µm Al foil, Norsk Hydro ASA, Oslo, Norway) with an areal capacity of 2.89 mAh/cm^2 and an apparent electrode density of 1.45 g/cm^3, whereas the active material of the negative electrode was coated onto Cu foil (11 µm Cu foil, Carl Schlenk AG, Roth, Germany) with an areal capacity of 3.25 mAh/cm^2 and an apparent electrode density of 1.03 g/cm^3. This leads to an N/P ratio of 1.12. To calculate the areal capacities, practical capacities of 200 and 350 mAh/g were taken for the active materials of the positive and negative electrode, respectively. After coating, the electrodes were dried overnight under vacuum and calendered (GK 300L, Saueressig Group, Vreden, Germany) yielding a target porosity of 40 %. The electrode sheets were then cut to disks with diameters of 15 mm for the positive electrodes and 16 mm for the negative electrodes, respectively. The electrode disks were then dried under vacuum at 80 °C for 12 h before transferring them into a glovebox (LabMaster Glove Box MB200-G, M. Braun, Garching, Germany) under Ar atmosphere (O_2 and $H_2O < 0.1$ ppm).

2.2. Cell preparation

2.2.1. Coin cells

Coin cells (CR2032) were prepared under Ar atmosphere using a 15 mm diameter positive electrodes, a 18 mm diameter negative electrodes, and Celgard 2500 separator (Celgard, Charlotte, North Carolina, USA) with a diameter of 19 mm and a thickness of 25 μm. 100 μL 1 M $LiPF_6$ in EC/DEC 1:1 (battery grade) with 1 wt% of VC (99.5 %, acid <200 ppm, H_2O < 100 ppm) or FEC (≥99 %, acid <200 ppm, anhydrous) were used as the electrolyte (all: Sigma Aldrich, St. Louis, Missouri; USA). In all cells, 1.1 mm wave springs and 1.5 mm spacers were used.

2.2.2. EL cells

For the gas analysis ECC DEMS Test Cells (EL-Cell, Hamburg, Germany) were used. The individual parts of the test cells were dried at 80 °C under vacuum for 12 h before transferring them to the glovebox. For these cells, a single Celgard 2500 separator was used with 150 μL of the electrolyte (1 M $LiPF_6$ in EC/DEC 1:1 and 1 wt% of the respective additive). To ensure a gastight system and a reproducible sampling procedure the test cell was connected via PEEK tubing (BGB Analytik, Boeckten, Switzerland) to electronically controllable membrane valves (Bürkert Austria GmbH, Mödling, Austria). A schematic test cell is shown in Fig. S2.

2.3. Characterization methods

2.3.1. Elemental surface composition by X-ray Photoelectron Spectroscopy

The coin cells were charged and discharged (CCCV) at ambient temperature using an Arbin BT-21084 (Arbin Instruments, College Station, Texas, USA) battery cycler. In one set of experiments, the cells were charged to 4.3 V at a C-rate of C/10, whereas in the second set, the cells were charged at C/10 to 4.3 V and then discharged to 3 V at the same rate. To prepare electrode samples for the XPS investigations, the coin cells were opened under inert atmosphere, and the extracted electrodes washed three times with DEC and fixed on a sample holder with carbon tape. All XPS measurements (Nexsa, ThermoFisher, Waltham, Massachusetts, USA) were performed with Al Kα radiation at 72 W and a pass energy of 50 and 200 eV for high-resolution and survey spectra, respectively. The spot size was 400 μm in "Standard Lens Mode" and CAE Analyser Mode with an integrated flood gun. The Avantage XPS software as provided by the manufacturer was used for the data analysis. The peaks were calibrated to adventitious carbon at 284.8 eV and the spectra deconvoluted with the Gaussian-Lorentzian model (GL(30)).

2.3.2. Operando gas chromatography mass spectrometry

The gas analysis was conducted with an in-house *operando* GC/MS system (see Fig. S3). The cells were connected to a SP-150 cycler (Bio-Logic, Grenoble, France) and a He supply of 10 mL/min flow. For sampling, the solenoid valves were electronically activated, and the gas sample was transferred to a 10-way GC valve connected to a 500 μL sample loop. In the loading position of the valve, the loop was filled with the sampled gas from the battery. Afterwards, the valve was switched, and the sample injected into the GC/MS instrument (Shimadzu GC/MS QP2010 SE, Shimadzu Corporation, Kyoto, Japan) via its split/splitless injector. The gas mixture was then separated in its components using a PLOT column (Rt-Q-BOND PLOT Column 30 m × 0.32 mm ID, 10 μm film, Restek Corporation, Centre County, Pennsylvania, USA) and analysed by mass spectrometry. Identification of individual compounds was achieved based on the comparison of their mass spectra with the entries in the NIST mass spectral library. After positive identification, a characteristic *m/z* signal was chosen for each gas species to monitor the species' concentration change over the whole experiment. The peak area was then normalized to the area of DEC. For every cell chemistry at least two experiments were performed, and the most representative experiment was used for comparison.

Table 2
Gas species found with *operando* GC/MS during the formation cycle with different cell chemistries. The reference (Ref) consists of an NMC811 vs. graphite and 1 M $LiPF_6$ EC/DEC 1:1 cell and for the additives 1 wt% of VC and FEC are added to the electrolyte, respectively. The gas species are sorted by their chemistry and the most significant *m/z* fragment is listed for each gas species.

Nr.	Name	*m/z* ratio	Chemistry	Ref	VC	FEC
1	Ethanol	31	Alcohol	x	x	x
2	Diethyl carbonate (DEC)	45	Carbonate	x	x	x
3	Dimethyl carbonate (DMC)	15	Carbonate	x	x	x
4	Ethylene carbonate (EC)	29	Carbonate	x	x	x
5	Ethyl methyl carbonate (EMC)	45	Carbonate	x	x	x
6	Vinylene carbonate (VC)	86	Carbonate		x	
7	Acetaldehyde	43	Carbonyl	x	x	x
8	Acetone	43	Carbonyl	x	x	x
9	Acetonitrile	41	Carbonyl	x	x	x
10	Ethyl acetate	43	Carbonyl	x	x	x
11	Ethyl formate	31	Carbonyl	x	x	x
12	Methyl formate	60	Carbonyl	x	x	x
13	1,3,5-Trioxane	61	Ether	x	x	x
14	1,3-Dioxolane	73	Ether	x	x	x
15	1,2-Dimethoxyethane	60	Ether	x	x	x
16	Ethyl ether	31	Ether	x	x	x
17	Furan	39	Ether	x	x	x
18	Fluoroethane	47	Fluoroalkane	x	x	x
19	2-Methyl-1-Propene	56	Hydrocarbon	x	x	x
20	Butane	43	Hydrocarbon	x	x	x
21	Cyclobutane	41	Hydrocarbon	x	x	x
22	Ethane	30	Hydrocarbon	x	x	x
23	Ethene	26	Hydrocarbon	x	x	x
24	Isobutane	43	Hydrocarbon	x	x	x
25	Methane	15	Hydrocarbon	x	x	x
26	Propane	43	Hydrocarbon	x	x	x
27	Propene	39	Hydrocarbon	x	x	x
28	Carbon dioxide	44	Carbon Oxide	x	x	x
29	Carbon monoxide	12	Carbon Oxide	x	x	x

2.3.3. Electrochemical testing

Long term cycling tests were performed with full cells on an Arbin BT-21084. For formation the cells were charged and discharged with a C-rate of C/10 after a resting time of 4 h with constant current constant voltage (CCCV) tests in a voltage window from 3.0 to 4.3 V. Subsequently, the long-term cycling behaviour was tested with 200 cycles of CCCV at a C-Rate of 1C.

3. Results and discussion

3.1. Overview gas analysis

The experiments were conducted by applying a general cycling protocol and a cell was charged and discharged (3.0 V–4.3 V vs. Li^+/Li) at a cycling rate of C/10. Before the first charge, a resting period of 4 h was applied. The cells were analysed with GC/MS and XPS once after completely charging the battery at the highest potential and once after discharge at the lowest potential (see Fig. S4). For the *operando* GC/MS set-up, the sampling process was optimized by automatically opening the electronically controllable valves when the desired potential was attained. Therefore, the formation process was not interrupted and the influence of the sampling procedure on the electrochemical measurement could be minimized. Therefore, one experimental set was used to depict gaseous decomposition products from the charge and discharge steps minimizing effects introduced by sample preparation. However, the XPS analyses were performed separately on the electrode materials in the charged (one charging step) and discharged (one charge followed by one discharge) states. In Fig. S4 the cell potential during the formation cycle is displayed including the points of sampling with GC/MS and XPS. Fig. S5 shows the potential curves of the investigated formation

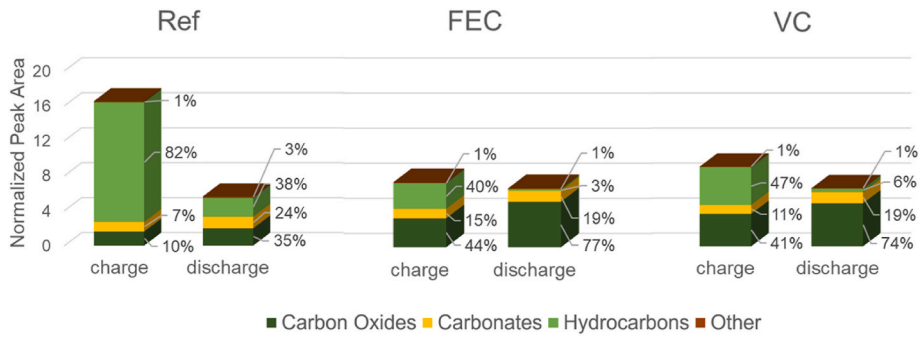

Fig. 1. Amount and distribution of gases organized according to their chemistry groups (see Table 2) during the formation cycle in a cell with NMC811 vs. graphite in 1 M $LiPF_6$ EC/DEC 1:1 without (Ref) and with 1 wt% additive (VC and FEC), charged and discharged with C/10.

cycle for all three cell chemistries. Additionally, the cells were tested with CCCV at a C-Rate of 1C for 200 cycles. As expected, minor effects of the SEI forming additives on the electrochemical performance were observed [27]. The discharge capacities and coulombic efficiencies can be found in Fig. S6. In general, the impact of SEI forming additives on the electrochemical performance of cells with graphite is smaller compared to cells with negative electrodes that are subjected to a larger volume expansion (e.g. Si or Si-Gr) [1,28–30]. Nonetheless, NMC811 vs. graphite served as a well-researched and stable system to mechanistically investigate the effect of SEI forming additives.

The gas phase consists of the original electrolyte components as well as the decomposition products from the formation cycle (see Fig. S7 and Table S1). 29 individual compounds were detected and grouped according to their chemistries and ordered alphabetically (see Table 2). For each gas species, the *m/z* ratio of the most significant fragment is given. Furthermore, the x in Table 2 indicates which gas species were identified for the given cell chemistry. The molecular structure of the additives is similar to the solvent molecules (EC and DEC, see Fig. S1) and resulted in the same decomposition products for all three cell chemistries. Regarding the cells with VC, the additive itself could also be identified even though only 1 wt% was present in the electrolyte. FEC on the other hand could not be identified due to the low peak intensities. For VC a significant mass was chosen from the fragmentation pattern to track the gas species despite its low intensity. Additional to the qualitative analysis, a semiquantitative analysis was performed on all 29 gas species and the results were compared regarding the state-of-charge (SOC) and the cell chemistry (see Fig. S8). The gas species which showed a distinct trend were included in the mechanistic discussion in the following sections.

Fig. 1 illustrates the distribution of the gas species organized in chemistry groups (see Table 2) and total gas amount evolved for each sampling point. In all investigated cells, more gas is produced during charge than in discharge. The reference cell (Ref) emits more than twice as much gaseous components in comparison to the cells with electrolyte additives. This result indicates that the use of electrolyte additives leads to a decrease in electrolyte decomposition. For both VC and FEC, the lowest unoccupied molecular orbital (LUMO) level lies below the main electrolyte components EC and DEC (see Fig. S9). Molecules with a low LUMO have a high electron affinity and subsequently a higher reduction tendency [31,32]. Therefore, the additives are preferentially reduced and decomposed prior to the main electrolyte components. A more stable SEI formed with VC and FEC can prevent further electrolyte decomposition [10–13].

The reference cell without any additive shows hydrocarbons as the dominant species with 82 % of the total gas amount during charge, compared to 40 % for FEC and 47 % for VC, and 38 % (Ref) compared to 6 % (VC) and 3 % (FEC) for discharge, respectively. Hydrocarbons are assumed to be a result of the decomposition of the main electrolyte components EC and DEC (see section 3.3.). Since the electrolyte additives decompose prior to the main electrolyte components due to a lower LUMO, a uniform SEI can be formed which inhibits the decomposition of EC and DEC.

The gas phase further consists of carbon oxides, in which carbon dioxide is the main contributor. The carbon oxides attain a concentration of 10 % in the charged state of the reference cell, whereas their concentrations are 44 and 41 % in the charged states of the cells with FEC and VC electrolyte additives, respectively. In the discharged state concentrations increase to 35 % for the reference compared to 77 and 74 % for the cells with FEC and VC additives, respectively. The fraction of carbon oxides in electrolytes with additives is more pronounced compared to the reference cell. This could indicate that carbon oxides are produced during decomposition of the electrolyte additives VC and FEC. This will be further discussed in section 3.2.1. The increase of carbon oxides from charge to discharge could be explained with the release of singlet oxygen at higher voltages. NMC materials have the tendency to release singlet oxygen ($^1O_2$) from the layered oxide structure at higher cell potentials and is reported for NMC at 4.3 V. The singlet oxygen can react with EC in the electrolyte to form CO and CO_2 (see Reaction 1) [33,34]. It can be assumed that during the constant voltage step NMC releases reactive oxygen species which result in increased carbon oxides levels when sampling after discharge.

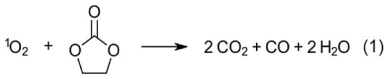

The residual gas phase is composed of carbonates and a small fraction of more complex gases including carbonyl species, ethers, alcohols and fluoroalkanes. The carbonates also increase from the charged state (7 % for Ref, 15 % for FEC and 11 % for VC) to the discharged state (24 % for Ref, 19 % for FEC and VC). As seen in Fig. S8, EC can only be detected after discharge. Since EC has a lower vapour pressure than DEC (0.0098 mm Hg at 25 °C for EC vs. 10.8 mm Hg at 25 °C for DEC [35,36]) the accumulation in the gas phase is shifted. The small fraction of residual gas species accounts for the remaining 1 % of the total gas phase except for the reference sample after discharge where this value is increased to 3 %.

3.2. Decomposition of VC and FEC

GC/MS data in conjunction with XPS data were used to gain further insights into the decomposition reactions of VC and FEC, and to compare these to a reference electrolyte without additive (Ref). The combination of these two methods allows a more thorough investigation of the electrolyte decomposition as the solid decomposition products on the electrode surfaces can be analysed with XPS, whereas the gaseous decomposition products can be monitored with the GC/MS.

3.2.1. Decomposition of VC

As already indicated in section 3.1., the amount of carbon dioxide

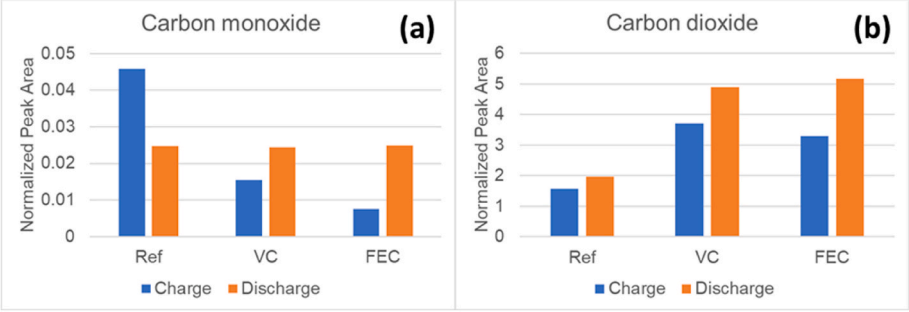

Fig. 2. Emission of carbon monoxide (a) and carbon dioxide (b) during formation with C/10 normalized to DEC in a cell with NMC811 vs. graphite in 1 M $LiPF_6$ EC/DEC 1:1 without (Ref) and with 1 wt% additive (VC and FEC).

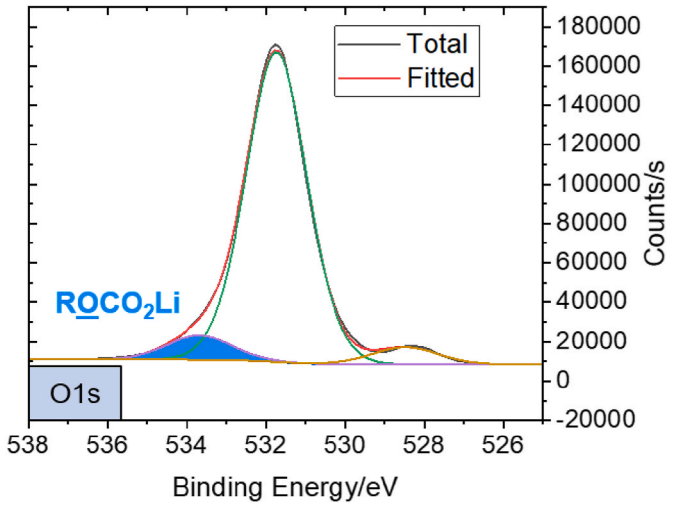

	Energy [eV]	Area [Counts]	Area [%]
Ref	533.5	16286	2.79
VC	533.7	25622	7.28
FEC	533.7	28711	7.30

Fig. 3. XPS spectra of the negative electrode showing the SEI layer after the first charge with C/10 for NMC811 vs. graphite in 1 M $LiPF_6$ EC/DEC 1:1 with 1 wt% additive (VC). This spectrum is representative for all measurements performed, i. e, with the reference electrolyte and with FEC. The absolute and relative peak areas of the respective sample of electrolytes are shown without (Ref) and with 1 wt% additive (VC and FEC), depicting an O1s spectrum.

produced for SEI forming additives is significantly higher than in the reference sample. Before going into further detail regarding the analysis of carbon dioxide it has to be mentioned that the decomposition of VC is also relevant for the decomposition of FEC since VC is formed from FEC by elimination of HF (see Reaction 2) [17,37]. However, among the two carbon oxides (CO and CO_2), CO is observed to be more prevalent in the reference cell (see Fig. 2). Both carbon oxides are side products of multiple decomposition reactions of the main electrolyte components EC and DEC. However, the direct decomposition of VC and of FEC via formation of VC produces only CO_2 and does not lead to CO (see Reaction 3) [10,17,37]. Fig. 2 succinctly confirms this, as more CO_2 is produced in the cells with VC and FEC electrolyte additives than in the reference cell. Since the electrolyte additives are decomposing prior to the main electrolyte components (see section 3.1.), a stable SEI is formed, and the main electrolyte components EC and DEC are decomposed to a lesser extent. This leads to a reduced CO production in the cells with electrolyte additives VC and FEC while the absence of a protective layer increases CO evolution (see Reaction 4) [38]. Additionally, formation of the methyl-radical from EC decomposition presents the origin of hydrocarbons which will be described below in section 3.

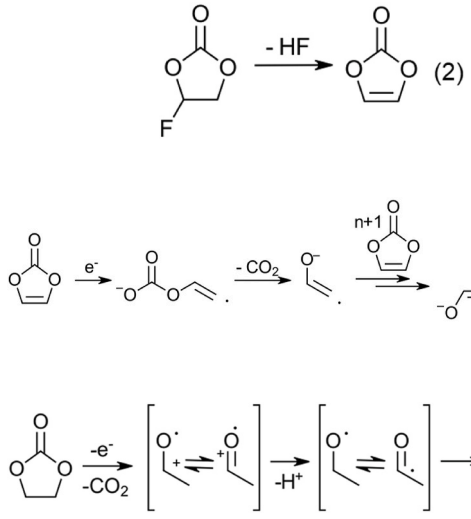

XPS, as a surface sensitive technique, allows the investigation of solid decomposition products originating from the electrolyte that deposits onto the electrode surfaces during formation. Fig. 3 shows the measured XPS spectrum of the surface of the negative electrode after first charge using VC as the electrolyte additive. This spectrum is representative of the data attained for all other negative electrode samples, i.e., measurements performed using the reference electrolyte and that with the FEC additive. Spectra for reference and VC can be found in the supporting information (see Fig. S10). For easier comparison of the peak areas, the absolute and the relative peak areas are listed in the table within Fig. 3. The peak in question is indicated in the spectrum of VC.

In the O1s spectrum a distinct peak reveals the existence of organic carbonate ($ROCO_2Li$) at 533.7 eV for the samples with VC and FEC [12]. Poly-VC is formed from VC (respectively from FEC by HF dissociation) and its repeating unit contains a carbonate. It is deposited onto the negative electrode to build a more flexible SEI compared to the main electrolyte components EC and DEC (see Reaction 3) [10,16]. $ROCO_2Li$ is also present in the reference sample but to a lesser extent since the decomposition of EC and DEC produces oligomers and polymers with carbonate species as terminal units. As a result, the peak area of O1s organic carbonate ($ROCO_2Li$) is smaller in the reference sample compared to VC and FEC (see Reaction 3 and Reaction 5) [7,8].

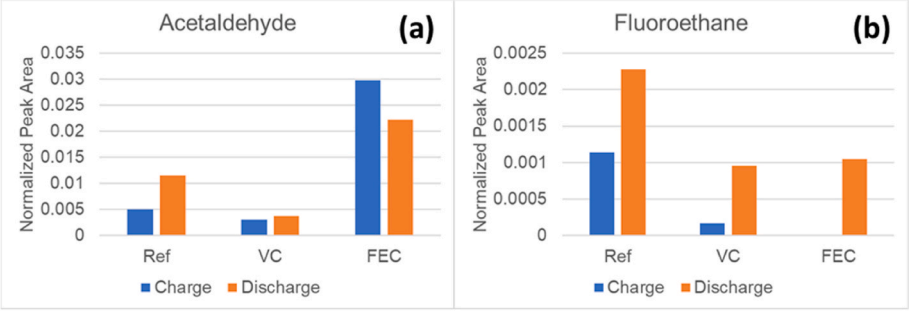

Fig. 4. Emission of acetaldehyde (a) and fluoroethane (b) during formation with C/10 normalized to DEC in a cell with NMC811 vs. graphite in 1 M $LiPF_6$ EC/DEC 1:1 without (Ref) and with 1 wt% additive (VC and FEC).

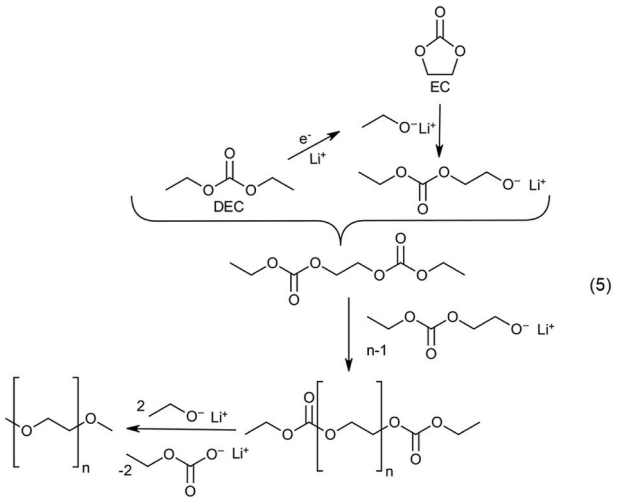

3.2.2. *Decomposition of FEC*

Although the chemical structures of FEC and VC are similar, it is still possible to observe a difference in their decomposition via gas analysis. Acetaldehyde is formed in larger quantities when FEC is decomposed compared to VC (Fig. 4a). The initialization of the polymerization reaction that leads to poly-VC can either be started from VC or directly from FEC (see Reaction 6a). During the initialization with FEC, the vinyloxy radical is formed as an intermediate, which can react to the vinyloxy radical anion by eliminating a proton. However, the elimination reaction that forms VC and HF from FEC likely increases the concentration of protons in an electrolyte with FEC. In this environment the elimination of a proton from the vinyloxy radical is less likely. Therefore, the concentration of the vinyloxy radical in cells with FEC is assumed to be higher than in cells with VC. In cells containing the FEC additive, acetaldehyde can be formed via a recombination reaction with a hydrogen radical (see Reaction 6b) [37,39]. This leads to an increased LiF content in the SEI upon SEI formation which will be discussed below in this section.

Fluoroethane contains a fluorine atom that does not stem from FEC but from the decomposition reaction of the conducting salt $LiPF_6$ (see Fig. 4b and Reaction 7) [40]. The content of fluoroethane is higher in the gas phase of the reference cell compared to the cells using VC and FEC. Since the SEI is less stable in the reference cell, repeated crack formation and exposure of fresh active material surfaces to the electrolyte can cause larger amounts of PF_5, thereby resulting in increased levels of fluorinated hydrocarbon compared to cells containing an additive. However, due to elevated fluoroethane concentrations some exposure of electrolyte to the electrodes can be assumed in electrolytes containing VC and FEC.

Table 3
Relative elemental ratios of F from XPS data of extracted NMC and graphite electrodes after charge and a full charge-discharge cycle.

Atom % F1s	Positive electrode		Negative electrode	
Electrolyte	Charge	Discharge	Charge	Discharge
Ref	13.82	18.44	8.92	14.58
VC	14.64	18.67	13.87	12.79
FEC	17.21	20.94	14.76	15.54

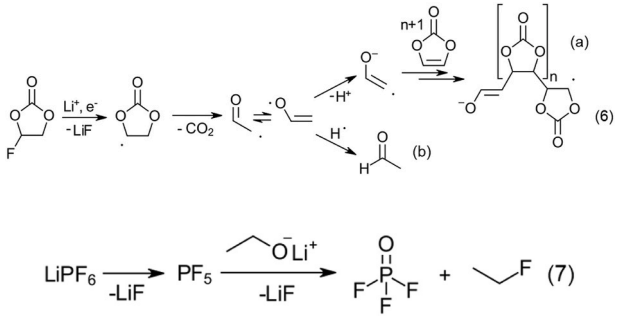

Table 3 shows the atomic percentage obtained of fluorine at the surface of the positive and negative electrode samples after charge and discharge using the three different electrolytes. This data was obtained from the evaluation of the elemental concentrations from the survey XPS spectrum. A significant amount of fluorine on the surfaces is assumed to originate from the decomposition of the conducting salt which also results in fluoroethane (see Reaction 7). The surplus of F in cells that contain FEC can be assigned to FEC decomposition leading also to LiF. This was observed on the positive as well as on the negative electrode, however, on the positive electrode it is more pronounced.

The C1s spectra and the F1s spectra (see Fig. 5) similarly reveal that the concentration of organic and inorganic fluorine species is higher for samples containing FEC. The spectrum of VC is representative of the data attained for all other electrode samples, i.e., measurements performed using the reference electrolyte and that with the FEC additive, for positive and negative electrode. Additional spectra can be found in the supporting information (see Figs. S11 and S12). Peak areas are presented in the table below the spectrum of VC to indicate the relevant peak (see Fig. 5). In the C1s spectrum the signal for $–CH_2CF_2-$ at 286 eV is higher for the samples containing FEC than in cells with VC or in the reference. The increased signal for $–CH_2CF_2-$ indicates that fluorine is incorporated into the polymer that forms the interphase [41].

A similar trend was observed in the F1s spectrum where the peak at 685.5 eV (LiF) is higher for electrodes cycled with FEC. LiF is primarily formed by the decomposition of $LiPF_6$ (see Reaction 7) [40]. However, LiF is also a side product of the decomposition of FEC into VC or acetaldehyde (see Reaction 6), stemming from active Li^+ trapped by HF to form LiF [17,37]. Therefore, the amount of fluoroethane in the gas phase

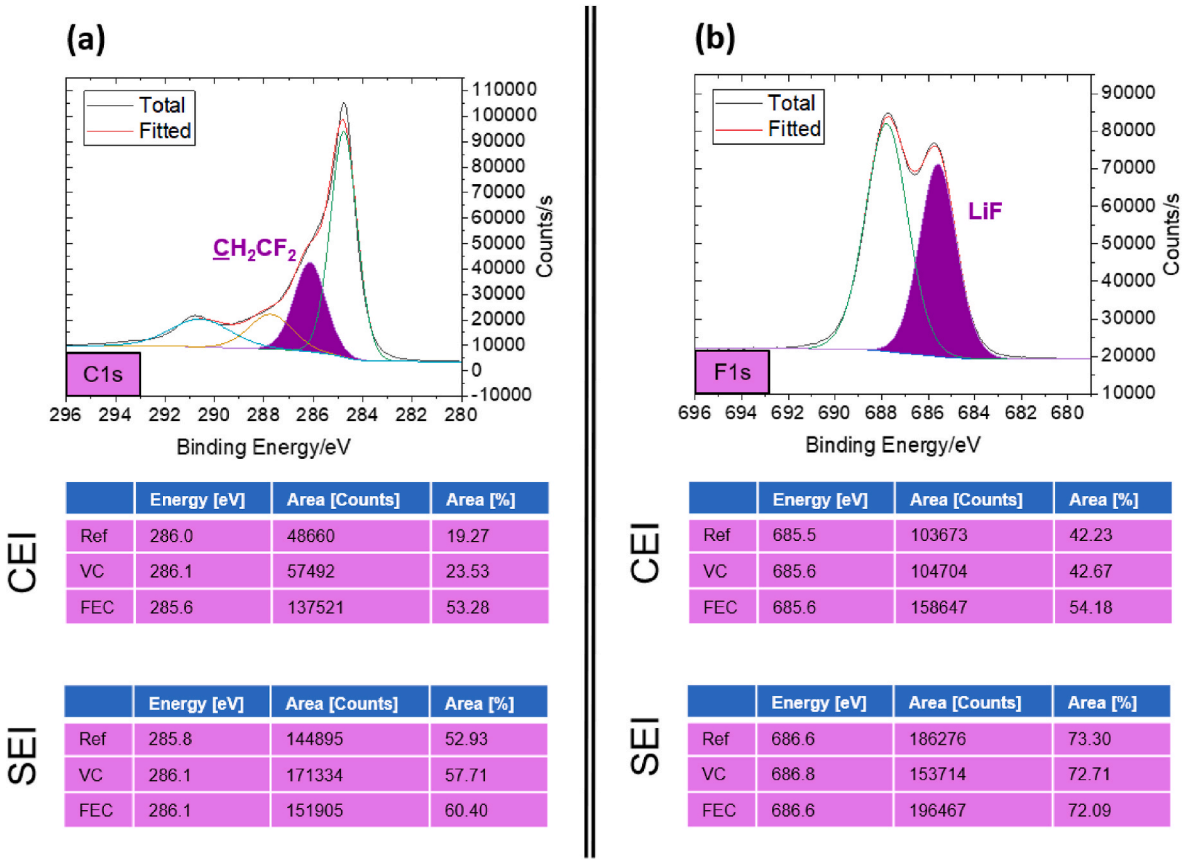

CEI

	Energy [eV]	Area [Counts]	Area [%]
Ref	286.0	48660	19.27
VC	286.1	57492	23.53
FEC	285.6	137521	53.28

SEI

	Energy [eV]	Area [Counts]	Area [%]
Ref	285.8	144895	52.93
VC	286.1	171334	57.71
FEC	286.1	151905	60.40

CEI

	Energy [eV]	Area [Counts]	Area [%]
Ref	685.5	103673	42.23
VC	685.6	104704	42.67
FEC	685.6	158647	54.18

SEI

	Energy [eV]	Area [Counts]	Area [%]
Ref	686.6	186276	73.30
VC	686.8	153714	72.71
FEC	686.6	196467	72.09

Fig. 5. XPS spectra of the positive electrode (CEI) after the first formation cycle with C/10 for NMC811 vs. graphite in 1 M $LiPF_6$ EC/DEC 1:1 with 1 wt% additive (VC). This spectrum is representative for all measurements performed, i. e, with the reference electrolyte and with FEC, for positive (CEI) and negative (SEI) electrode. The absolute and relative peak areas of the respective sample of electrolytes are shown without (Ref) and with 1 wt% additive (VC and FEC), depicting a C1s spectrum for the organic fluorine species (a) and a F1s spectrum for the inorganic fluorine species (b); for both spectra the relative areas are presented in the table below.

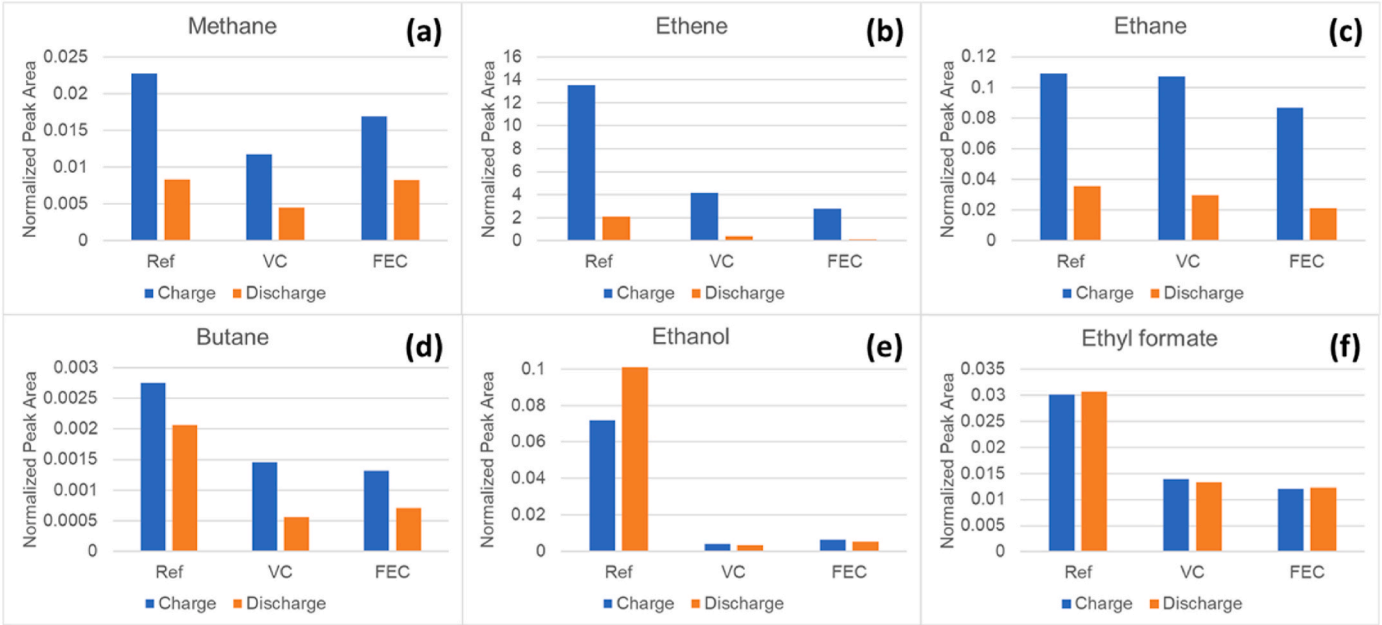

Fig. 6. Gas emission during formation with C/10 for gas species indicative of the decomposition of EC and DEC: hydrocarbons (methane (a), ethene (b), ethane (c), butane (d)), ethanol (e) and ethyl formate (f) normalized to DEC in a cell with NMC811 vs. graphite in 1 M $LiPF_6$ EC/DEC 1:1 without (Ref) and with 1 wt% additive (VC and FEC).

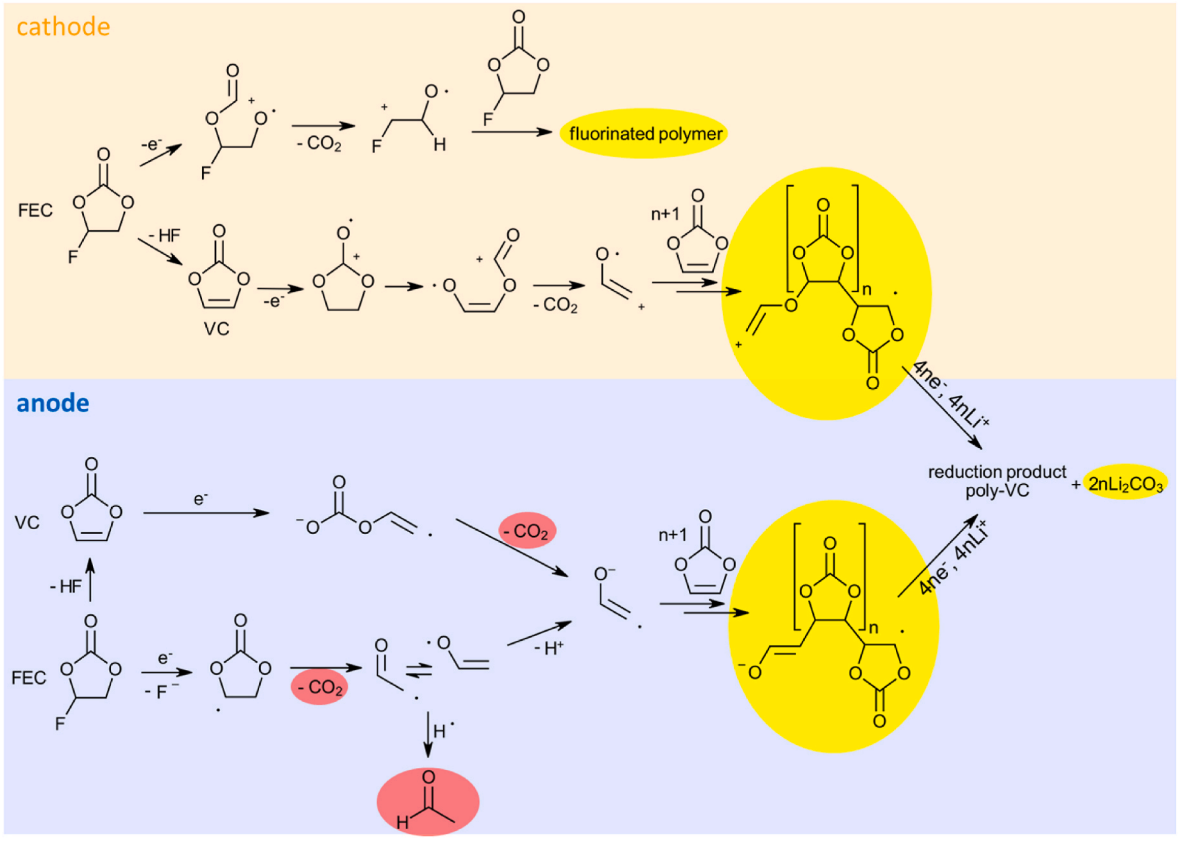

Fig. 7. Summary of the decomposition reactions of FEC and VC.

is larger in the reference stemming from increased $LiPF_6$ decomposition due to an insufficiently protective SEI layer. On the electrode surfaces, there is a divergence in the LiF content on the positive and the negative electrode (see Fig. 5). The CEI on the positive electrode shows a clear increase of LiF with the use of FEC as electrolyte additive, which correlates with increased acetaldehyde values (see Figs. 4 and 5 and Reaction 6). The SEI on the other hand does not follow the same trend. It has to be noted that the detection of surface layers employing XPS is limited by the penetration depth of this technique which accounts only for up to 5 nm into the material [19,40] but remains sufficient to depict the CEI (1–5 nm) [12,19]. However, reported thickness of the SEI varies between 10 nm and 100 nm which poses a challenge for XPS [1,16]. Therefore, the elevated F values from FEC decomposition are more pronounced on the positive electrode.

3.3. Decomposition of EC and DEC

It was expected that the SEI and the gas phase in cells with VC and FEC mainly consists of decomposition products derived from the additives rather than from the main electrolyte components, primarily EC. Therefore, larger amounts of e.g. ethene, a decomposition product of the base electrolyte, are observed in the reference cell [10]. Such decomposition reactions form volatile organic compounds (VOCs) which can be monitored with *operando* GC/MS.

Fig. 6 shows the gas species that are mainly indicative of the decomposition of EC and DEC as the main electrolyte solvents. Hydrocarbons are a major indicator of the decomposition of the main electrolyte solvents which are represented by methane, ethene, ethane and butane (see Reactions 8, 9, 12 and 13). However, it was discovered that monitoring the decomposition of EC and DEC is not limited to only hydrocarbons since ethanol and ethyl formate are also predominantly formed in the reference cell (see Reaction 10).

Ethene (see Fig. 6b) is directly formed from the electrochemical decomposition of EC (see Reaction 8) [40]. During SEI formation, EC is predominantly decomposed compared to the linear carbonate (in this case DEC). Therefore ethene as the primary decomposition product in the gas phase has the largest contribution to hydrocarbons [42].

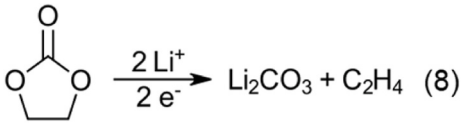

However, some gas species are lacking on reported decomposition pathways that connects them to EC. Therefore, gas species like ethanol, butane and ethyl formate can only be explained by a reaction mechanism deriving from DEC (see Fig. 6d–f). The formation reaction of butane is similar to ethene, a direct electrochemical decomposition of DEC (see Reaction 9) [43].

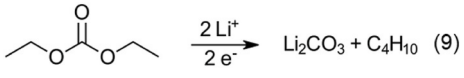

A single electron reduction of DEC on the other hand can lead to a bond cleavage within the carbonate unit to yield lithium ethanolate and the carboxylate radical. The carboxylate radical further reacts in a recombination reaction with a hydrogen radical to form ethyl formate. Lithium ethanolate reacts with the traces of water present in the electrolyte to form ethanol and lithium hydroxide (see Reaction 10) [40]. There is a notable difference in the signal intensity of ethanol between the reference and the cells containing electrolyte additives which can be explained by the scavenging effect of VC (also from FEC decomposition) on the ethanolate (see Reaction 11) [44,45].

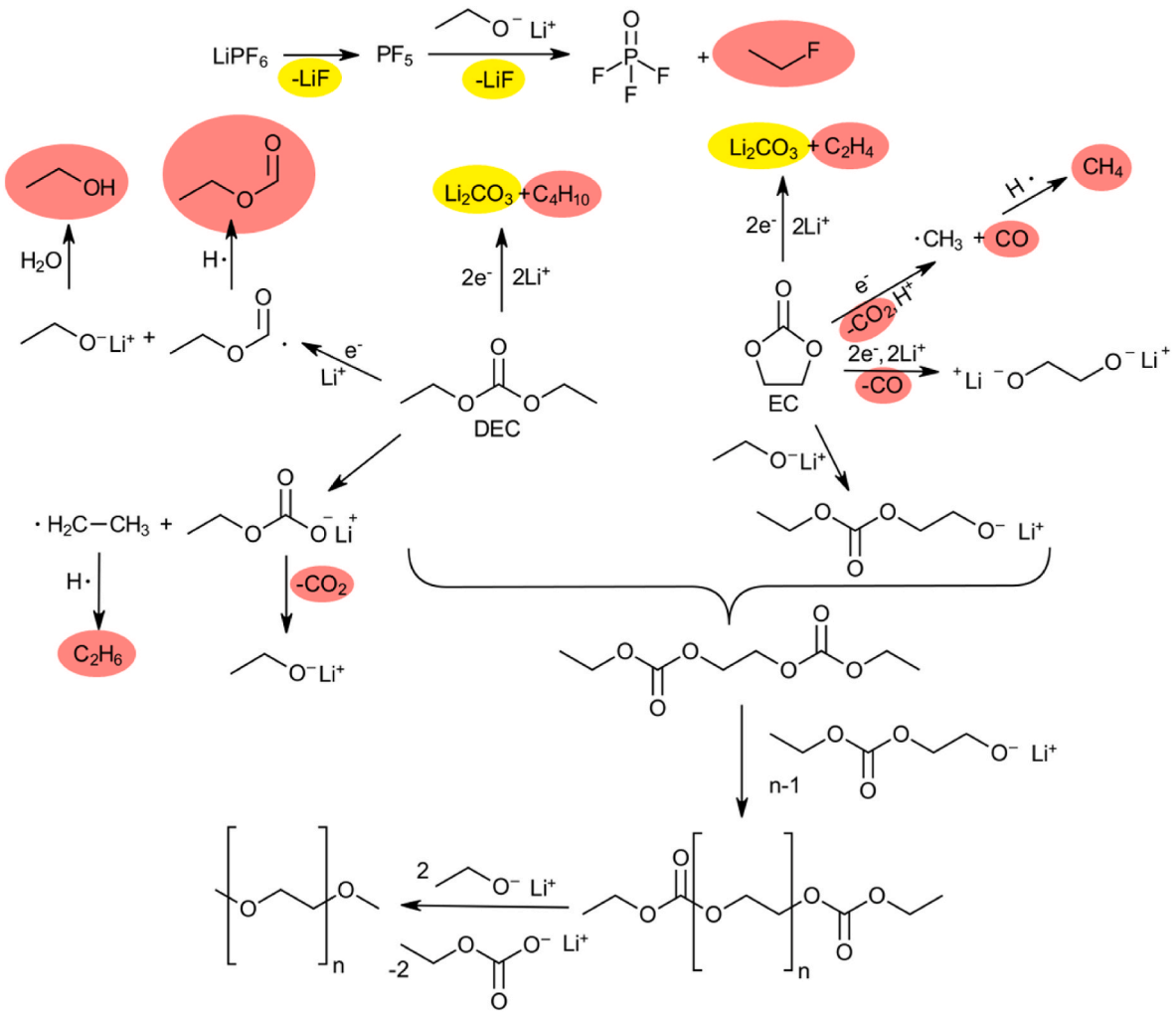

Fig. 8. Summary of the decomposition reactions of the main electrolyte components EC and DEC.

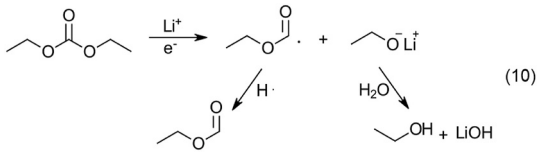

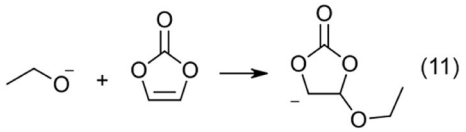

Lastly, methane and ethane (see Fig. 6a and c) are the result of radical recombination reactions. The different radical fragments originate from atom transfer reactions of radicals initiated by electrochemical means within the highly reactive environment of the electrolyte during cell operation (see Reactions 12 and 13) [46,47].

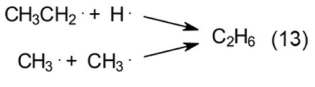

However, the intensity of the methane signal is much lower than with an electrolyte containing DMC or EMC, where the methyl radical can be the result of the electrochemical breakdown of both the linear carbonate or the cyclic carbonate [38]. In the electrolyte described in this paper, the methyl-radical stems only from the cyclic carbonate as DEC only produces ethyl radicals (see Reaction 4 in section 3.2.1.).

Figs. 7 and 8 provide a summary of the decomposition reactions that are observed in the cells investigated in this work. Fig. 7 illustrates the decomposition of the additives, whereas Fig. 8 exemplifies the breakdown of the main electrolyte components.

4. Conclusion

In this work, operando GC/MS supported by XPS was used to identify gaseous and electrolyte-electrode interphase components that form when SEI stabilizing VC and FEC are used at concentrations as low as 1 wt%. For cells containing electrolyte additives, carbon oxides were the main decomposition product in the gas phase. Carbon dioxide in particular exhibited a higher concentration in cells with VC and FEC than in the reference cell. In contrast, the formation of carbon monoxide points to the decomposition of the main electrolyte solvent components (EC and DEC), linking the formation of carbon monoxide to the decomposition of the base electrolyte. This is supported by XPS data which shows an increase in organic carbonate components on the electrode surface of additive-containing cells. The composition of the electrode surface showed that the addition of FEC resulted in a higher fluorine content in the SEI and CEI which was reflected in the respective

C1s and F1s spectra. The decomposition of FEC can also be investigated by monitoring the concentration of acetaldehyde in the gas phase, which is formed during the polymerization of FEC.

The analysis of the gas phase after electrochemical cycling showed a larger hydrocarbon signal for the reference compared to the cells cycled with electrolyte additives. This is particularly pronounced during charge and is reflected in the total amounts as well as in the concentration of the individual hydrocarbon species such as methane, ethane, ethene and butane. Additional identified gas species, such as ethanol, ethyl formate, and fluoroethane can be linked to the decomposition of the base electrolyte. Ethanol showed a particularly pronounced signal in the cell with the reference electrolyte, which appeared significantly lower in electrolytes with additives and can be explained by scavenging effects of VC removing alkoxides from the mixture.

This work demonstrates the capability of time-resolved measurements employing an *operando* GC/MS system to investigate the evolution of gaseous compound in correlation to the SOC, which supports the investigation of degradation mechanisms of the base electrolyte, and any additives present even in small quantities. Gas analysis in conjunction with solid state analytical techniques applied to the electrode surfaces, i.e., XPS, has proven to give a comprehensive picture of SEI formation and the concurrent degradation reactions of the base electrolyte and its additives.

CRediT authorship contribution statement

Christiane Groher: Writing – original draft, Visualization, Validation, Software, Methodology, Investigation, Formal analysis, Data curation. **Damian Marlon Cupid:** Writing – review & editing, Supervision. **Andreas Mautner:** Writing – review & editing, Data curation. **Erwin Rosenberg:** Writing – review & editing, Supervision. **Jürgen Kahr:** Writing – review & editing, Writing – original draft, Validation, Supervision, Project administration, Methodology, Investigation, Funding acquisition, Formal analysis, Data curation, Conceptualization.

Declaration of competing interest

The authors declare that they have no known competing financial interests or personal relationships that could have appeared to influence the work reported in this paper.

Data availability

Data will be made available on request.

Acknowledgement

This research was carried out at the Battery Material Laboratory at AIT Austrian Institute of Technology GmbH and the work was supported by the FFG (Austrian Research Promotion Agency) within the project No. 879613.

Appendix A. Supplementary data

Supplementary data to this article can be found online at https://doi.org/10.1016/j.jpowsour.2024.234481.

References

[1] M. Armand, P. Axmann, D. Bresser, M. Copley, K. Edström, C. Ekberg, et al., Lithium-ion batteries – current state of the art and anticipated developments, J. Power Sources 479 (2020) 228708, https://doi.org/10.1016/j.jpowsour.2020.228708.

[2] B. Scrosati, History of lithium batteries, J. Solid State Electrochem. 15 (7–8) (2011) 1623–1630, https://doi.org/10.1007/s10008-011-1386-8.

[3] M.V. Reddy, A. Mauger, C.M. Julien, A. Paolella, K. Zaghib, Brief history of early lithium-battery development, Materials 13 (8) (2020) 1–9, https://doi.org/10.3390/MA13081884.

[4] J. Dahn, U. von Sacken, M. Juzkow, H. Al-Janaby, Rechargeable LiNiO 2/carbon cells, J. Electrochem. Soc. 138 (8) (1991) 2207–2211, https://doi.org/10.1149/1.2085950.

[5] R. Fong, U. von Sacken, J. Dahn, Studies of lithium intercalation into carbons using nonaqueous electrochemical cells, J. Electrochem. Soc. 137 (7) (1990) 3–7, https://doi.org/10.1149/1.2086855.

[6] A. Wang, S. Kadam, H. Li, S. Shi, Y. Qi, Review on modeling of the anode solid electrolyte interphase (SEI) for lithium-ion batteries, npj Comput. Mater. 4 (1) (2018), https://doi.org/10.1038/s41524-018-0064-0.

[7] T. Sasaki, T. Abe, Y. Iriyama, M. Inaba, Z. Ogumi, Formation mechanism of alkyl dicarbonates in Li-ion cells, J. Power Sources 150 (1–2) (2005) 208–215, https://doi.org/10.1016/j.jpowsour.2005.02.021.

[8] G. Gachot, S. Grugeon, M. Armand, S. Pilard, P. Guenot, J.M. Tarascon, et al., Deciphering the multi-step degradation mechanisms of carbonate-based electrolyte in Li batteries, J. Power Sources 178 (1) (2008) 409–421, https://doi.org/10.1016/j.jpowsour.2007.11.110.

[9] S.J. An, J. Li, C. Daniel, D. Mohanty, S. Nagpure, D.L. Wood, The state of understanding of the lithium-ion-battery graphite solid electrolyte interphase (SEI) and its relationship to formation cycling, Carbon N. Y. (2016) 10552–10576, https://doi.org/10.1016/j.carbon.2016.04.008.

[10] D. Pritzl, S. Solchenbach, M. Wetjen, H.A. Gasteiger, Analysis of vinylene carbonate (VC) as additive in graphite/LiNi0.5Mn1.5O4 cells, J. Electrochem. Soc. 164 (12) (2017) A2625–A2635, https://doi.org/10.1149/2.1441712jes.

[11] Y. Qian, P. Niehoff, M. Börner, M. Grützke, X. Mönnighoff, P. Behrends, et al., Influence of electrolyte additives on the cathode electrolyte interphase (CEI) formation on LiNi1/3Mn1/3Co1/3O2 in half cells with Li metal counter electrode, J. Power Sources (2016) 32931–32940, https://doi.org/10.1016/j.jpowsour.2016.08.023.

[12] Y. Qian, C. Schultz, P. Niehoff, T. Schwieters, S. Nowak, F.M. Schappacher, et al., Investigations on the electrochemical decomposition of the electrolyte additive vinylene carbonate in Li metal half cells and lithium ion full cells, J. Power Sources (2016) 33260–33271, https://doi.org/10.1016/j.jpowsour.2016.09.100.

[13] S. Chen, H. Che, F. Feng, J. Liao, H. Wang, Y. Yin, et al., Poly(vinylene carbonate)-based composite polymer electrolyte with enhanced interfacial stability to realize high-performance room-temperature solid-state sodium batteries, ACS Appl. Mater. Interfaces 11 (46) (2019) 43056–43065, https://doi.org/10.1021/acsami.9b11259.

[14] W. Liu, J. Li, W. Li, H. Xu, C. Zhang, X. Qiu, Inhibition of transition metals dissolution in cobalt-free cathode with ultrathin robust interphase in concentrated electrolyte, Nat. Commun. 11 (1) (2020), https://doi.org/10.1038/s41467-020-17396-x.

[15] B.S. Parimalam, A.D. MacIntosh, R. Kadam, B.L. Lucht, Decomposition reactions of anode solid electrolyte interphase (SEI) components with LiPF, J. Phys. Chem. C 121 (41) (2017) 22733–22738, https://doi.org/10.1021/acs.jpcc.7b08433.

[16] M. Nie, J. Demeaux, B.T. Young, D.R. Heskett, Y. Chen, A. Bose, et al., Effect of vinylene carbonate and fluoroethylene carbonate on SEI formation on graphitic anodes in Li-ion batteries, J. Electrochem. Soc. 162 (13) (2015) A7008–A7014, https://doi.org/10.1149/2.0021513jes.

[17] V. Etacheri, O. Haik, Y. Goffer, G.A. Roberts, I.C. Stefan, R. Fasching, et al., Effect of fluoroethylene carbonate (FEC) on the performance and surface chemistry of Si-nanowire li-ion battery anodes, Langmuir 28 (1) (2012) 965–976, https://doi.org/10.1021/la203712s.

[18] S. Grugeon, P. Jankowski, D. Cailleu, C. Forestier, L. Sannier, M. Armand, et al., Towards a better understanding of vinylene carbonate derived SEI-layers by synthesis of reduction compounds, J. Power Sources 427 (February) (2019) 77–84, https://doi.org/10.1016/j.jpowsour.2019.04.061.

[19] K. Edström, T. Gustafsson, J.O. Thomas, The cathode-electrolyte interface in the Li-ion battery, Electrochim. Acta 50 (2004) 397–403, https://doi.org/10.1016/j.electacta.2004.03.049, 2-3 SPEC. ISS.

[20] S.S. Zhang, A review on electrolyte additives for lithium-ion batteries, J. Power Sources 162 (2006) 1379–1394, https://doi.org/10.1016/j.jpowsour.2006.07.074, 2 SPEC. ISS.

[21] Y. Zhou, M. Su, X. Yu, Y. Zhang, J.G. Wang, X. Ren, et al., Real-time mass spectrometric characterization of the solid–electrolyte interphase of a lithium-ion battery, Nat. Nanotechnol. 15 (3) (2020) 224–230, https://doi.org/10.1038/s41565-019-0618-4.

[22] B. Rowden, N. Garcia-Araez, A review of gas evolution in lithium ion batteries, Energy Rep. (2020) 610–618, https://doi.org/10.1016/j.egyr.2020.02.022.

[23] J.-P. Schmiegel, M. Leißing, F. Weddeling, F. Horsthemke, J. Reiter, Q. Fan, et al., Novel in situ gas formation analysis technique using a multilayer pouch bag lithium ion cell equipped with gas sampling port, J. Electrochem. Soc. 167 (6) (2020) 060516, https://doi.org/10.1149/1945-7111/ab8409.

[24] N. Tsiouvaras, S. Meini, I. Buchberger, H.A. Gasteiger, A novel on-line mass spectrometer design for the study of multiple charging cycles of a Li-O 2 battery, J. Electrochem. Soc. 160 (3) (2013) A471–A477, https://doi.org/10.1149/2.042303jes.

[25] R. Jung, M. Metzger, F. Maglia, C. Stinner, H.A. Gasteiger, Oxygen release and its effect on the cycling stability of LiNi x Mn y Co z O 2 (NMC) cathode materials for Li-ion batteries, J. Electrochem. Soc. 164 (7) (2017) A1361–A1377, https://doi.org/10.1149/2.0021707jes.

[26] K.N. Shitaw, S.C. Yang, S.K. Jiang, C.J. Huang, N.A. Sahalie, Y. Nikodimos, et al., Decoupling interfacial reactions at anode and cathode by combining online electrochemical mass spectroscopy with anode-free Li-metal battery, Adv. Funct. Mater. 31 (6) (2021) 1–12, https://doi.org/10.1002/adfm.202006951.

[27] R.D. Deshpande, P. Ridgway, Y. Fu, W. Zhang, J. Cai, V. Battaglia, The limited effect of VC in graphite/NMC cells, J. Electrochem. Soc. 162 (3) (2015) A330–A338, https://doi.org/10.1149/2.0221503jes.
[28] K. Feng, M. Li, W. Liu, A.G. Kashkooli, X. Xiao, M. Cai, et al., Silicon-based anodes for lithium-ion batteries: from fundamentals to practical applications, Small 14 (2018) 8, https://doi.org/10.1002/smll.201702737.
[29] C.M. Park, J.H. Kim, H. Kim, H.J. Sohn, Li-alloy based anode materials for Li secondary batteries, Chem. Soc. Rev. 39 (8) (2010) 3115–3141, https://doi.org/10.1039/b919877f.
[30] X. Zuo, J. Zhu, P. Müller-Buschbaum, Y.J. Cheng, Silicon based lithium-ion battery anodes: a chronicle perspective review, Nano Energy 31 (November 2016) (2017) 113–143, https://doi.org/10.1016/j.nanoen.2016.11.013.
[31] H Bin Son, M.Y. Jeong, J.G. Han, K. Kim, K.H. Kim, K.M. Jeong, et al., Effect of reductive cyclic carbonate additives and linear carbonate co-solvents on fast chargeability of LiNi0.6Co0.2Mn0.2O2/graphite cells, J. Power Sources 400 (May) (2018) 147–156, https://doi.org/10.1016/j.jpowsour.2018.08.022.
[32] H. Haruna, S. Takahashi, Y. Tanaka, Accurate consumption analysis of vinylene carbonate as an electrolyte additive in an 18650 lithium-ion battery at the first charge-discharge cycle, J. Electrochem. Soc. 164 (1) (2017) A6278–A6280, https://doi.org/10.1149/2.0441701jes.
[33] R. Jung, M. Metzger, F. Maglia, C. Stinner, H.A. Gasteiger, Chemical versus electrochemical electrolyte oxidation on NMC111, NMC622, NMC811, LNMO, and conductive carbon, J. Phys. Chem. Lett. 8 (19) (2017) 4820–4825, https://doi.org/10.1021/acs.jpclett.7b01927.
[34] B.L.D. Rinkel, J.P. Vivek, N. Garcia-Araez, C.P. Grey, Two electrolyte decomposition pathways at nickel-rich cathode surfaces in lithium-ion batteries, Energy Environ. Sci. (2022) 153416.
[35] PubChem Compound Summary for CID 7303, Ethylene carbonate, National Center for Biotechnology Information. [Online]. Available: https://pubchem.ncbi.nlm.nih.gov/compound/Ethylene-carbonate.
[36] PubChem Compound Summary for CID 7766, Diethyl carbonate, National center of biotechnology information [Online]. Available: https://pubchem.ncbi.nlm.nih.gov/compound/Diethyl-carbonate.
[37] A.L. Michan, B.S. Parimalam, M. Leskes, R.N. Kerber, T. Yoon, C.P. Grey, et al., Fluoroethylene carbonate and vinylene carbonate reduction: understanding lithium-ion battery electrolyte additives and solid electrolyte interphase formation, Chem. Mater. 28 (22) (2016) 8149–8159, https://doi.org/10.1021/acs.chemmater.6b02282.
[38] M. Metzger, B. Strehle, S. Solchenbach, H.A. Gasteiger, Origin of H2 evolution in LIBs: H2O reduction vs. Electrolyte oxidation, J. Electrochem. Soc. 163 (5) (2016) A798–A809, https://doi.org/10.1149/2.1151605jes.
[39] Y. Jin, N.J.H. Kneusels, P.C.M.M. Magusin, G. Kim, E. Castillo-Martínez, L. E. Marbella, et al., Identifying the structural basis for the increased stability of the solid electrolyte interphase formed on silicon with the additive fluoroethylene carbonate, J. Am. Chem. Soc. 139 (42) (2017) 14992–15004, https://doi.org/10.1021/jacs.7b06834.
[40] G. Gachot, P. Ribière, D. Mathiron, S. Grugeon, M. Armand, J.B. Leriche, et al., Gas chromatography/mass spectrometry as a suitable tool for the li-ion battery electrolyte degradation mechanisms study, Anal. Chem. 83 (2) (2011) 478–485, https://doi.org/10.1021/ac101948u.
[41] L. Xia, B. Tang, L. Yao, K. Wang, A. Cheris, Y. Pan, et al., Oxidation decomposition mechanism of fluoroethylene carbonate-based electrolytes for high-voltage lithium ion batteries: a dft calculation and experimental study, ChemistrySelect 2 (24) (2017) 7353–7361, https://doi.org/10.1002/slct.201700938.
[42] A. Kriston, I. Adanouj, V. Ruiz, A. Pfrang, Quantification and simulation of thermal decomposition reactions of Li-ion battery materials by simultaneous thermal analysis coupled with gas analysis, J. Power Sources 435 (2019) 226774, https://doi.org/10.1016/j.jpowsour.2019.226774.
[43] R. Dedryvère, H. Martinez, S. Leroy, D. Lemordant, F. Bonhomme, P. Biensan, et al., Surface film formation on electrodes in a LiCoO2/graphite cell: a step by step XPS study, J. Power Sources 174 (2) (2007) 462–468, https://doi.org/10.1016/j.jpowsour.2007.06.033.
[44] T. Sasaki, T. Abe, Y. Iriyama, M. Inaba, O. Zempachi, Suppression of an alkyl dicarbonate formation in suppression of an alkyl dicarbonate formation in Li-ion cells, J. Electrochem. Soc. 152 (10) (2005) A2046–A2050, https://doi.org/10.1149/1.2034517.
[45] Y. Liu, S. Takeda, I. Kaneko, H. Yoshitake, T. Mukai, M. Yanagida, et al., Understanding the improved high-temperature cycling stability of comprehensive analysis approach utilizing LC-MS and DART-MS, J. Phys. Chem. C (2018) 1225864–1225870, https://doi.org/10.1021/acs.jpcc.7b10391.
[46] C.T. Avedisian, W.C. Kuo, W. Tsang, A. Lowery, High temperature thermal decomposition of diethyl carbonate by pool film boiling, 140:6, https://doi.org/10.1115/1.4038572, 2018.
[47] B. Yamada, P. Zetterlund, General chemistry of radical polymerization, in: K. Matyjaszewski, P. Thomas (Eds.), Handbook of Radical Polymerization, John Wiley and Sons, Hoboken, 2003, pp. 117–186.